Journal of
Synchrotron
Radiation

ISSN 1600-5775

Received 5 May 2014
Accepted 6 June 2014

Ronchi test for characterization of X-ray nanofocusing optics and beamlines

Fredrik Uhlén,[a]* Jussi Rahomäki,[a] Daniel Nilsson,[a] Frank Seiboth,[b] Claude Sanz,[a] Ulrich Wagner,[c] Christoph Rau,[c,d,e] Christian G. Schroer[b] and Ulrich Vogt[a]

[a]Biomedical and X-ray Physics, KTH Royal Institute of Technology, Stockholm 106 91, Sweden, [b]Institute of Structural Physics, Technische Universität Dresden, Dresden 01062, Germany, [c]Diamond Light Source Ltd, Diamond House, Harwell Science and Innovation Campus, Didcot, Oxfordshire OX11 0DE, UK, [d]School of Materials, University of Manchester, Manchester M1 7HS, UK, and [e]Department of Otolaryngology, Northwestern University School of Medicine, Chicago, IL 60611, USA. *E-mail: fredrik.uhlen@biox.kth.se

A Ronchi interferometer for hard X-rays is reported in order to characterize the performance of the nanofocusing optics as well as the beamline stability. Characteristic interference fringes yield qualitative data on present aberrations in the optics. Moreover, the visibility of the fringes on the detector gives information on the degree of spatial coherence in the beamline. This enables the possibility to detect sources of instabilities in the beamline like vibrations of components or temperature drift. Examples are shown for two different nanofocusing hard X-ray optics: a compound refractive lens and a zone plate.

Keywords: zone plate; compound refractive lens; Ronchi interferometer.

1. Introduction

X-ray imaging with nanofocused X-ray beams is a rapidly growing area at modern synchrotron radiation facilities. X-ray radiation from an undulator source is focused to very small spot sizes in the 10–100 nm-diameter range, and exciting applications can be found in many fields of science, ranging from physics, chemistry and material science to earth science and environmental science, to biology, medicine and life science. This development is technologically driven by the ability to manufacture better X-ray optics with higher spatial resolution and the construction of new synchrotron radiation sources with an ever-increasing brilliance, like the NSLS II or MAX IV facilities. In this paper we present the Ronchi test as a simple and fast method to characterize the focusing performance of both beamline and nanofocusing optics.

Although the detailed optical design of existing and future nanofocusing beamlines differs from case to case, they all follow the same basic construction idea. A large distance between source and nanofocusing optic ensures that the latter is illuminated with spatial coherent light leading to a diffraction-limited focal spot. However, it is still a challenging task to manufacture nanofocusing optics that indeed are diffraction-limited, *i.e.* aberration-free. Recent fabrication developments have focused on four major types of optics: Kirkpatrick–Baez mirrors, nanofocusing lenses, zone plates and multilayer-Laue lenses.

Independent of the specific optical device chosen for nanofocusing, the optical characterization of nanofocusing optics has emerged as an important task to ensure expected focal spot sizes can be reached in reality. Indeed, a large variety of different wavefront measuring tools have been developed in recent years, including, but not limited to, Hartmann wavefront sensors (Flöter *et al.*, 2010), pencil beam deflectometers (Hignette *et al.*, 1997), speckle trackers (Bérujon *et al.*, 2012), grating-based interferometers (Weitkamp *et al.*, 2005) and ptychography (Schropp *et al.*, 2010; Kewish *et al.*, 2010*a*,*b*; Vila-Comamala *et al.*, 2011; Hönig *et al.*, 2011).

Even with an aberration-free nanofocusing optics it can sometimes be difficult to reach down to the focal spot sizes expected by the diffraction limit. The reason lies often in instabilities of other optical components placed between source and final optics, like monochromator and beam-steering mirrors. A common example is vibrations induced by cooling of a certain device, which will result in a reduced spatial coherence and an increased final focus size. Vibrations could also be present in the experimental station itself, between optics and sample. Moreover, temperature drifts at the experimental station can also deteriorate the final resolution of X-ray images obtained by scanning microscopy.

In this paper we present the classical Ronchi test as a fast and simple method to qualitatively characterize both nanofocusing optics and the performance of a whole nanofocusing beamline. Originally introduced in the X-ray range at a free-electron laser source (Nilsson *et al.*, 2012), we believe the method is also ideally suited for X-ray imaging beamlines at modern synchrotron radiation facilities that want to achieve nanometer-sized focal spots. As examples we show the characterization of a nanofocusing compound refractive lens and a

large-diameter zone plate. Moreover, we present how the Ronchi test could be used to pinpoint the source of vibrations in beamline components and explain how the stability of the focused beam at the sample position can be monitored.

2. Ronchi test

The Ronchi test was developed by the Italian physicist Vasco Ronchi in the 1920s in order to characterize telescope lenses and mirrors. It was shown early on that the method is very sensitive to third-order aberrations and comparing acquired data with reference image tables was a quick and easy way to characterize aberrations instead of other time-consuming methods such as the Hartmann test at that time. The cheap and simple arrangement of the Ronchi method has since then been an appreciated tool in visible optics metrology (Ronchi, 1963).

The experimental arrangement is essentially a shearing interferometer (see Fig. 1). Optics under investigation focus light onto a grating positioned close to the focus. The grating splits the incoming light into different diffraction orders, which overlap on a detector placed further downstream. If the transverse spatial coherence is high enough, *i.e.* coherence over half the optic diameter, the first orders can be separated by choosing a grating period $d = \lambda/\mathrm{NA}$ (λ is the wavelength of the light and NA the numerical aperture of the optic) so that they only interfere with the zeroth order. The interference between the two orders results in a clear and characteristic fringe pattern, also called a Ronchigram. For a diffraction-limited optic the fringe pattern will appear as straight lines parallel to the grating orientation when placing the grating slightly before or after the focal point on the optical axis. However, if the wavefront behind the optic deviates from a spherical wave due to aberrations, the fringe pattern will appear deformed. This deformation is very characteristic of a certain type of aberration and by a visual inspection of the fringes it is possible to obtain a qualitative idea about the wavefront deformation. Examples of different characteristic Ronchigrams for common third-order aberrations can be seen in Fig. 1.

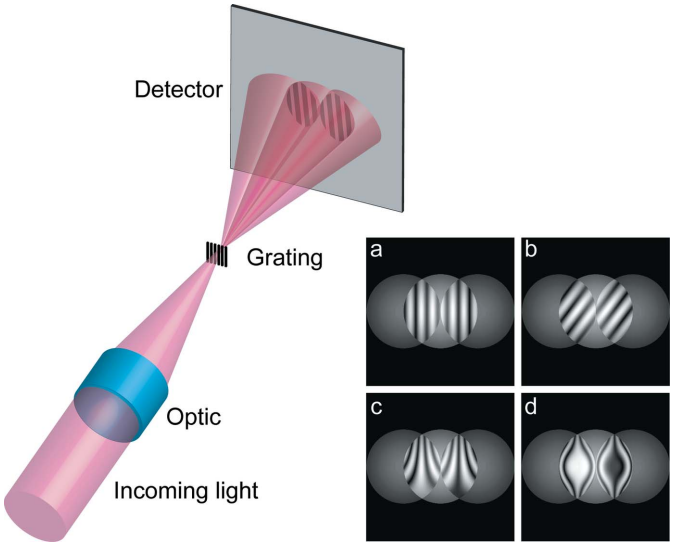

Figure 1
Experimental arrangement of a Ronchi interferometer. The grating is placed at or close to the focus. To the right: examples of Ronchigrams for different cases: (*a*) aberration-free optic, (*b*) astigmatism, (*c*) coma and (*d*) spherical aberration.

3. Experiment at Diamond Light Source

The experiment was performed at the coherence branch of I13 beamline at Diamond Light Source, UK (Rau *et al.*, 2011). A photon energy of 8.5 keV was chosen by a monochromator. The vertical coherence length is given by the source size, meaning the height of the electron beam, which is 6 µm (RMS). In the horizontal direction a slit placed 22 m downstream from the undulator was set to a 50 µm gap.

We investigated two different X-ray nanofocusing optics: a compound refractive lens (CRL) and a large-diameter zone plate (ZP). The CRL consisted of 30 single beryllium lenses with a radius of curvature of 50 µm, resulting in an overall focal length of 182 mm. The lenses were kept in helium atmosphere in order to avoid the formation of beryllium oxide during operation. An additional 300 µm aperture was positioned in front of the lenses. The second optic was a 500 µm-diameter tungsten ZP with 100 nm outermost zone width and 500 nm tungsten thickness, placed on a 100 µm-thick diamond substrate. The focal length was 334 mm. This optic had been previously characterized at a free-electron laser, but only with a single grating orientation (Nilsson *et al.*, 2012). This is not ideal because aberrations that are parallel to the grating line cannot be detected. For our experiments we therefore always used two gratings with vertical and horizontal orientation.

The grating sample was fabricated in 1 µm tungsten placed on 100 µm diamond substrate. This gives an approximate $\pi/2$ phase shift for 8.5 keV X-ray photons, which results in close to optimum contrast in the Ronchigram (0.64π phase shift is required for the zeroth and first diffraction order to be equally strong in intensity). The sample consisted of a grating matrix with horizontal and vertical orientations, respectively, and periods ranging from 100 nm to 310 nm. During the experiment, the sample was positioned in the vicinity of the focus of the lenses. By translating the sample in and out of focus along the optical axis, a series of Ronchigrams were recorded for each type of optics in both the horizontal and vertical direction. A grating period of 200–210 nm was required in order to obtain optimal overlap between the zeroth and first diffraction order.

As high-resolution X-ray detector we used a 150 µm-thick $CdWO_4$ scintillator that was imaged with a microscope objective with five times magnification onto a Manta 145B camera with 6.45 µm × 6.45 µm pixels. The effective pixel size was 1.3 µm and the resolution ∼3 µm. Exposure time was set to 5 s. The detector was placed approximately 200 mm downstream from the focus of the nanofocusing lenses, making the whole experimental arrangement very compact.

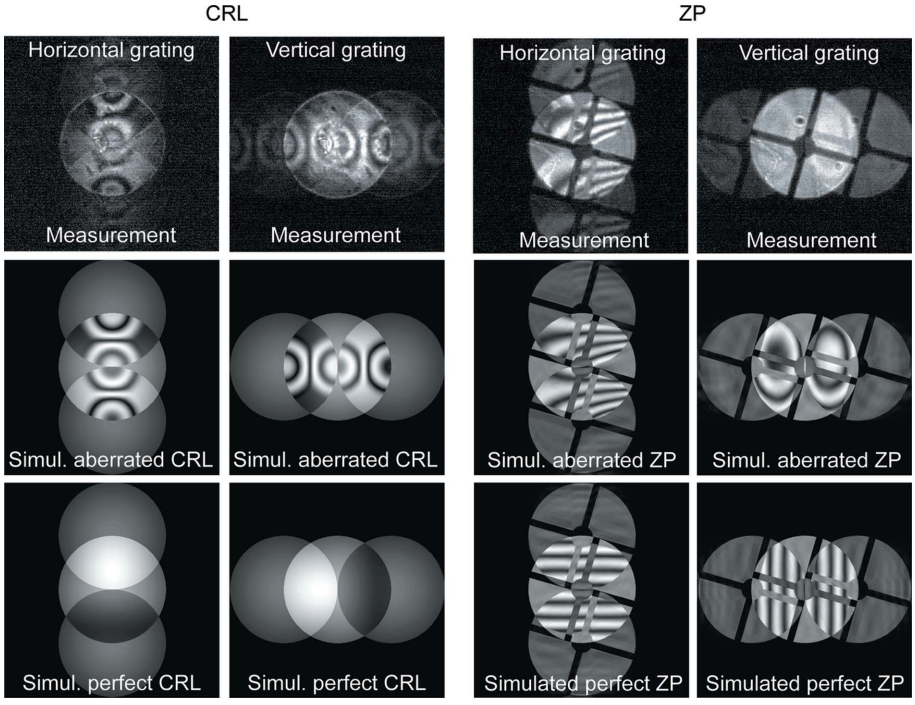

Figure 2
Top row: measured Ronchigrams with horizontal and vertical gratings, using a CRL (0 mm defocus) on the left side and a ZP (−1.0 mm defocus) on the right. Middle row: simulated Ronchigrams with aberrations. Bottom row: simulated Ronchigrams for perfect aberration-free optics. The cross in the right-hand-side images is the ZP central stop.

In order to further investigate measured Ronchigrams with respect to possible aberrations present, we developed a simulation tool in MATLAB which can simulate Ronchigrams for different X-ray optics. The optic is defined by an aperture transmission function along with the focal length. Grating input parameters include period, phase shift, orientation and position on the optical axis. Aberrations are defined as optical path differences (OPD) in the aperture plane. A simulated Ronchigram is then easily obtained by wavefront propagation methods based on Fourier transforms.

4. Characterization of nanofocusing X-ray optics

Fig. 2 shows measured Ronchigrams in the horizontal and vertical directions for both CRL (left) and ZP (right) together with simulated Ronchigrams. In the CRL example the grating was positioned in the focal plane. In this case the Ronchigram for an ideal aberration-free CRL should show no fringes as displayed in the lowest row of Fig. 2. Instead, characteristic circular fringes were visible. For the ZP example a grating positioned 1 mm before the focal plane was chosen. For an ideal zone plate this should result in straight fringes as shown in the lowest row in Fig. 2. In reality, curved fringes were observed, with a distinct difference between the two grating orientations. This gives already an indication of the presence of astigmatism.

For a better idea about the type and cause of the observed aberrations, the simulation tool was used to calculate Ronchigrams as similar as possible to the measured data. The simulated Ronchigrams are shown in the middle row of Fig. 2, and the corresponding OPDs introduced in the aperture plane are shown in Fig. 3 (top row).

The simulated wavefront aberration of the CRL is rotationally symmetric and perhaps best described as spherical aberration in the centre of the lens. The peak value is estimated to 1.5λ. The cause for this aberration is imperfec-

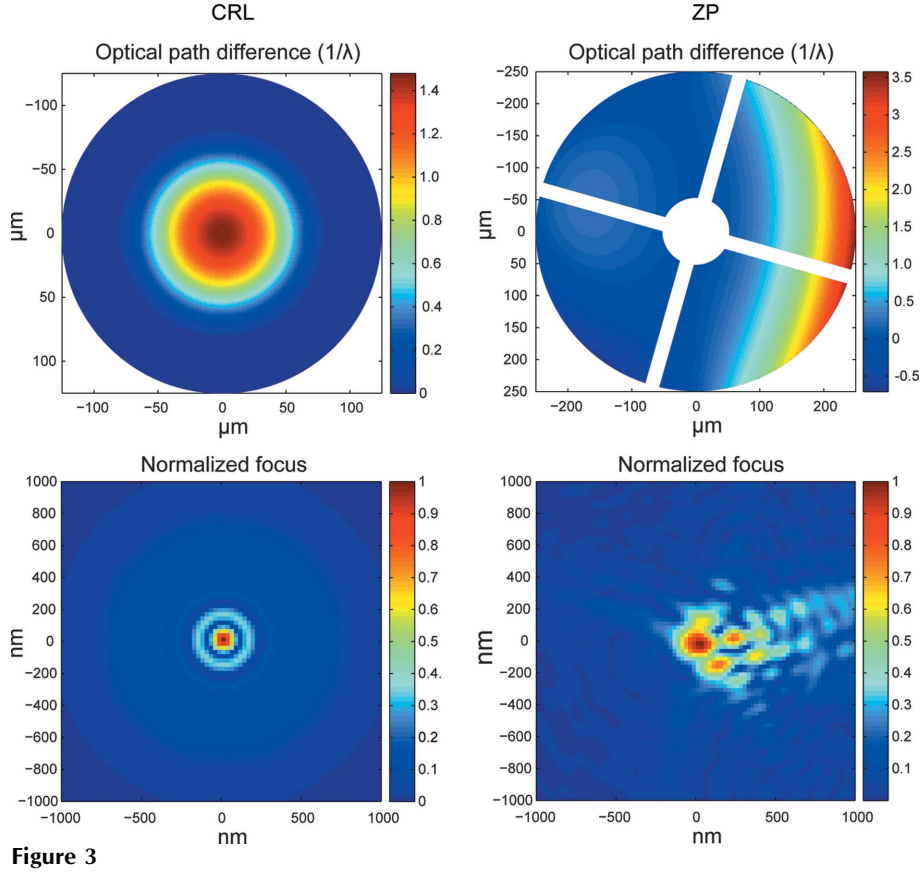

Figure 3
Top row: optical path differences (CRL left, ZP right) in the aperture function that gives the simulated Ronchigrams shown in Fig. 2 (middle row). Bottom row: corresponding simulated focal spots in the nominal focal plane. Amplitude is displayed.

tions in the fabrication process of the individual lenses. The lenses are fabricated by pressing the beryllium material to form a parabolic lens shape. However, the fabricated form deviates from the ideal shape in the middle of the lens, resulting in a slightly smaller radius of curvature than intended and a shorter paraxial focal length. This agrees well with ptychographic reconstructions and Fourier-based analysis of data recorded during the same beam time (Rahomäki *et al.*, 2014).

For the ZP, the aberrations consist of 1.8λ peak astigmatism in 80° and 2λ peak coma in 100°. This result agrees well with previous measurement at LCLS (Nilsson *et al.*, 2012). The aberrations are again due to a manufacturing imperfection, in this case writing of the zone plate pattern using an e-beam lithography tool. Inaccuracies in the interferometric laser-stage movement render an ellipsoidal shape of the zone plate and stage-position drift during a long exposure time results in non-concentric zone rings. The former error results in astigmatism and the latter in coma.

A Fourier transform of the aberrated transmission functions can give an idea about the expected focal spot shapes in the nominal focal plane, as displayed in the bottom row of Fig. 3. The CRL focal spot exhibits distinct side lobes with high amplitude. The ZP focal spot has a very complex shape, where the focus is spread out in a coma-like tail but also in other directions due to astigmatism and the presence of the central stop.

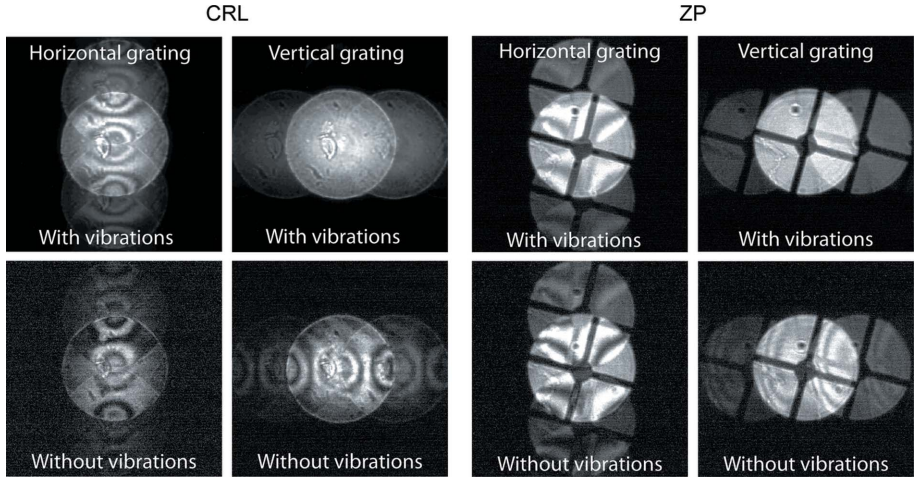

Figure 4
Top row: Ronchigrams with horizontal and vertical gratings for CRL (left) and ZP (right) at the beginning of the experiment with vibrations present. Bottom row: Ronchigrams without vibrations.

5. Effect of beamline instabilities and temperature drift on Ronchigrams

As mentioned above, the Ronchi test presented here needs good spatial coherence over an area that corresponds to about half the optic diameter. Lower spatial coherence will result in a lower visibility of the fringe pattern. In the following we will show how this was used to investigate and pinpoint beamline instabilities.

At the beamline I13, optics, such as the mirror or monochromator, are only horizontally deflecting. Therefore any coherence degradation should not occur in the vertical direction but only in the horizontal. This can be observed as shown in Fig. 4 (top row). A source of vibration, here the cooling for the monochromator, deteriorated the degree of coherence in the horizontal direction but not in the vertical. When eliminating this vibration source, also the coherence in the horizontal direction is re-established with the zone plate, which can be directly observed in the Ronchigram in Fig. 4 (right, bottom row). With the CRL, however, only after an improvement of the CRL stage did the fringes finally appear also in this case. This experience shows the strong potential of the Ronchi test to give information not only about the optic but also about the stability of the beamline and experiment components.

Another point to note is that the Ronchi test, as any other interferometer, is very sensitive to position changes of its components. A reason for this could be temperature drift at the experimental station. Thus a Ronchigram carries important stability information about the experimental arrangement consisting of optic and sample. If the illuminated area on the grating is changed, *i.e.* relative drift between lens and grating position, the interference minima and maxima in the Ronchigram change position accordingly. Hence, a drift of approximately a tenth of a period is easily discernible, especially if the Ronchigram contains only few fringes. That means that for our experiment a drift of 20 nm is detectable. This information is vital when performing experiments that require long-term stability, *e.g.* scanning procedures.

6. Summary

In this paper we presented the classical Ronchi test using hard X-ray synchrotron radiation for the characterization of nanofocusing X-ray optics and beamlines. Measured Ronchigrams revealed aberrations in two different nanofocusing optics: a CRL and a ZP. Simulations could qualitatively describe the type and magnitude of the aberrations. Moreover, the Ronchi test could be used to pinpoint vibrations in beamline components.

The main advantage of the Ronchi test is the simple experimental arrangement, only a grating sample and an X-ray detector are needed, and the easy visual inspection of measured Ronchigrams. No calculations are needed to obtain a qualitative idea about the performance of optics and beamline. The test can be used for a wide range of X-ray energies and both with synchrotron and free-electron laser radiation.

The authors gratefully acknowledge the financial support of the Swedish Science Research Council, the Swedish Foundation for Strategic Research, the Göran Gustafsson Foundation, the Wallenberg Foundation, the European Community's Seventh Framework Programme (FP7/2007–2013) under Grant No. 226716, and the German Ministry of Education and Research (BMBF) grants 05K13OD2 and 05K13OD4. The experiment was performed at the coherence branch of I13 beamline at Diamond Light Source, UK.

References

Bérujon, S., Ziegler, E., Cerbino, R. & Peverini, L. (2012). *Phys. Rev. Lett.* **108**, 158102.

Flöter, B., Juranić, P., Kapitzki, S., Keitel, B., Mann, K., Plönjes, E., Schäfer, B. & Tiedtke, K. (2010). *New J. Phys.* **12**, 083015.

Hignette, O., Freund, A. & Chinchio, E. (1997). *Proc. SPIE*, **3152**, 188–199.

Hönig, S., Hoppe, R., Patommel, J., Schropp, A., Stephan, S., Schöder, S., Burghammer, M. & Schroer, C. G. (2011). *Opt. Express*, **19**, 16325–16329.

Kewish, C. M., Guizar-Sicairos, M., Liu, C., Qian, J., Shi, B., Benson, C., Khounsary, A. M., Vila-Comamala, J., Bunk, O., Fienup, J. R., Macrander, A. T. & Assoufid, L. (2010). *Opt. Express*, **18**, 23420–23427.

Kewish, C. M., Thibault, P., Dierolf, M., Bunk, O., Menzel, A., Vila-Comamala, J., Jefimovs, K. & Pfeiffer, F. (2010). *Ultramicroscopy*, **110**, 325–329.

Nilsson, D., Uhlén, F., Holmberg, A., Hertz, H. M., Schropp, A., Patommel, J., Hoppe, R., Seiboth, F., Meier, V., Schroer, C. G., Galtier, E., Nagler, B., Lee, H. J. & Vogt, U. (2012). *Opt. Lett.* **37**, 5046–5048.

Rahomäki, J., Uhlén, F., Seiboth, F., Sanz, C., Nilsson, D., Lundström, L., Wagner, U., Schroer, C. G. & Vogt, U. (2014). In preparation.

Rau, C., Wagner, U., Pesic, Z. & De Fanis, A. (2011). *Phys. Status Solidi A*, **208**, 2522–2525.

Ronchi, V. (1963). *Appl. Opt.* **3**, 437–451.

Schropp, A., Boye, P., Feldkamp, J. M., Hoppe, R., Patommel, J., Samberg, D., Stephan, S., Giewekemeyer, K., Wilke, R. N., Salditt, T., Gulden, J., Mancuso, A. P., Vartanyants, I. A., Weckert, E., Schöder, S., Burghammer, M. & Schroer, C. G. (2010). *Appl. Phys. Lett.* **96**, 091102.

Vila-Comamala, J., Diaz, A., Guizar-Sicairos, M., Mantion, A., Menzel, A., Kewish, C. M., Bunk, O. & David, C. (2011). *Opt. Express* **19**, 21333–21344.

Weitkamp, T., Nöhammer, B., Diaz, A., David, C. & Ziegler, E. (2005). *Appl. Phys. Lett.* **86**, 054101.